

A new astronomical timescale for the loess deposits of Northern China

D. Heslop*, C.G. Langereis, M.J. Dekkers

Fort Hoofddijk Paleomagnetic Laboratory, Budapestlaan 17, 3584 CD Utrecht, The Netherlands

Received 14 July 2000; received in revised form 19 October 2000; accepted 20 October 2000

Abstract

Here, we present a refined timescale for the entire sequence of Quaternary Chinese loess, which relies upon the correlation of detailed monsoon records to the astronomical solution of Laskar (1990) and the oceanic ODP677 $\delta^{18}\text{O}$ record of Shackleton et al. (1990). The chronological scheme considers in detail the relative structures of the palaeoclimatic and palaeomagnetic records to produce an accurate timescale that is consistent with the current understanding of loess depositional and post-depositional processes. Analysis of this chronological framework demonstrates downward displacement of the palaeomagnetic horizons with respect to the climatic record. © 2000 Elsevier Science B.V. All rights reserved.

Keywords: loess; monsoons; cyclic processes; insolation; Loess Plateau; Quaternary

1. Introduction

The loess deposits of Northern China (33–47°N, 75–127°E, Fig. 1) act as a key archive in the study of palaeoclimatic change. Investigation of the loess sequences has led to the development of a number of continuous palaeoclimatic records through the utilisation of physical parameters demonstrated to be accurate proxies for variations in the East Asian monsoon system over the past 2.6 Myr.

The loess and intercalated palaeosol units provide a clear record of climatic shifts between the domination of glacial (winter) and interglacial

(summer) type monsoon states. The relatively unweathered sediments of the lightly coloured loess units are characteristic of dust accumulation under the cold and dry conditions of the East Asian winter monsoon system. Palaeosols are darker in colour and formed by weathering of the loessic dust, a pedogenic process driven by the warm and moist conditions of the summer monsoon [3].

A number of proxy parameters have been developed in an effort to extract climatically sensitive data from Chinese loess sequences (see [4] for a review). Zhou et al. [5] proposed that the increases in magnetic low field susceptibility (χ) detected in palaeosol units could be (at least partially) attributed to the formation of fine-grained magnetic minerals (magnetite and/or maghaemite) as a product of the pedogenic process. A number of studies have demonstrated a close correspond-

* Corresponding author. Fax: +31-30-2531677;
E-mail: heslop@geo.uu.nl

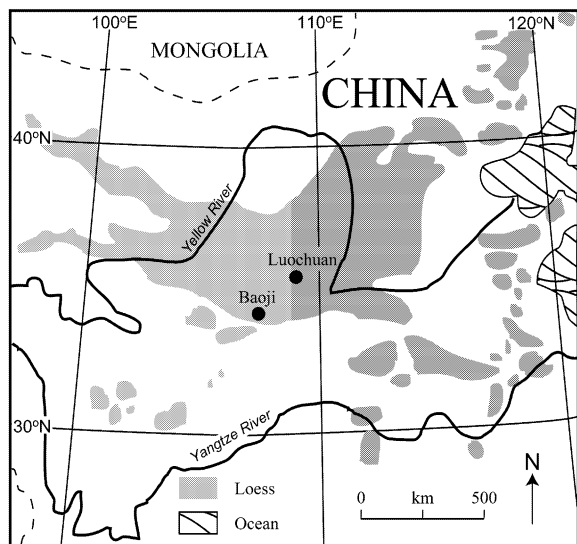


Fig. 1. Map displaying the pattern of loess distribution within China and the site locations utilised in this study.

ence in the χ variations within Chinese loess sequences to signatures of past global climatic change derived from other archives, e.g. oceanic and ice-core $\delta^{18}\text{O}$ profiles [6–8]. The link between the magnetic parameters of the loess sequences and climate has led to the use of magnetic susceptibility as a primary indicator of past summer monsoon activity.

Loess grain size is closely controlled by the magnitude of the winter monsoon winds that are responsible for the transport of aeolian dust into Northern China, with stronger monsoon winds resulting in the transport of larger sediment particles [4]. Ding et al. [9] utilised a number of absolute grain size parameters and particle size ratios to reconstruct past winter monsoon intensity for the entire Quaternary loess sequence at Baoji.

1.1. Astronomical timescales

The construction of palaeoclimatic records from oceanic archives has demonstrated that since the appearance of major glaciations in the Northern Hemisphere, global ice volume (defined by $\delta^{18}\text{O}$) has varied on a rhythmical basis. The cyclical nature of the oceanic $\delta^{18}\text{O}$ signal allowed climatic variations to be calibrated in time via the

association of identified isotopic oscillations to orbitally controlled changes in insolation [10–12]. Tuning of the cyclical palaeoclimatic profiles to the known orbital periods of eccentricity (125 and 95 kyr), obliquity (54 and 41 kyr) and climatic precession (quasi-periods 23 and 19 kyr) has thus proved to be a powerful tool in the construction of chronological models. Orbital tuning ordinarily takes place in the time domain and involves a process of correlation of the studied geological profile to computed variations in the positions of the Earth's rotational axis and orbital path. Such an astronomical correlation relies on initially fitting the longer period geological features to the insolation record and gradually increasing the resolution of the proposed fit by the further correlation of higher frequency features. Orbital tuning has been utilised in the production of high-resolution astrochronologies for both oceanic sediments [2,13] and continental sequences [9,14–16].

1.2. Astronomical solutions for the Chinese loess

Recently, Ding et al. [9] (hereafter referred to as DYRL₉₄) constructed an orbital scheme for grain size variations recorded in the Baoji section, whilst Lu et al. [16] (hereafter referred to as LLZAD₉₉) formulated an orbital age model for the magnetic susceptibility profile of the Luochuan section.

There are a number of apparent inconsistencies in the construction of the DYRL₉₄ and LLZAD₉₉ age models that result in substantial chronological inaccuracies. Both models utilised palaeomagnetic boundaries to provide key reference ages both in the formulation of preliminary lithologically dependent age models and for comparative purposes to test the robustness of the tuned timescale. The reference ages, utilised in the DYRL₉₄ solution are now known to be inaccurate, with more recently published dates demonstrating that the ages are in error by as much as ~ 120 kyr (Table 1). Although the LLZAD₉₉ model utilises ages closer to the accepted boundary dates (Table 1), both it and the DYRL₉₄ model are inconsistent in their treatment of the relative relationship of the palaeomagnetic and palaeoclimatic archives. In a

Table 1

Palaeomagnetic reversal reference ages utilised by this study [2,18,29,30], the study of Ding et al. [9] and the study of Lu et al. [16]

Reversal	DYRL ₉₄ control age (Ma)	LLZAD ₉₉ control age (Ma)	HLD ₀₀ control age (Ma)	<i>i-cycle</i> <i>code</i>	DYRL ₉₄ (Ma)	Δ age (kyr)	LLZAD ₉₉ (Ma)	Δ age (kyr)	Baoji HLD ₀₀ (Ma)	Δ age (kyr)	Luochuan HLD ₀₀ (Ma)	Δ age (kyr)
M/B	0.730 [33]	0.780 [34]	0.778 [29]	73	0.751	−27	0.769	−9	0.804	26	0.801	23
J/M	0.920 [33]	0.984 [34]	0.990 [2]	93	0.935	−55	0.946	−44	0.996	6	1.037	47
M/J	0.970 [33]	1.049 [34]	1.070 [2]	99–100	0.987	−83	1.001	−69	1.053	−17	1.113	43
O/M	1.670 [33]	1.757 [34]	1.785 [18]	174	1.668	−117	1.710	−75	1.800	15	1.803	18
M/O	1.870 [33]	1.983 [34]	1.942 [18]	187–188	1.882	−60	1.951	9	1.958	16	1.961	19
G/M	2.480 [33]	2.600 [34]	2.582 [30]	249–250	2.487	−95	2.630	48	2.603	21	2.602	20

Determined reversal ages are shown for the DYRL₉₄, LLZAD₉₉ and HLD₀₀ orbital models with the loess–reference age difference shown as ‘ Δ age’ (positive age values correspond to a downward displacement of the palaeomagnetic signal as would be expected in the formation of a delayed NRM).

study of the Luochuan section, Zhou and Shackleton [17] demonstrated the presence of a downwardly displaced natural remanent magnetisation (NRM) with respect to the palaeoclimatic record. A process of delayed NRM lock-in would result in the diachronous formation of the palaeoclimatic and palaeomagnetic archives. Both the DYRL₉₄ and LLZAD₉₉ schemes construct orbital models under the assumption that parallel points in their palaeomagnetic and palaeoclimatic records are isochronal. Therefore their final models often produce reversal ages that are more recent than the accepted boundary age, a scenario that is untenable according to the downward NRM displacement phenomena [17].

By attempting to provide the best one-to-one correlation between the loess and astronomical data sets both the DYRL₉₄ and LLZAD₉₉ schemes appear in places to be inconsistent with respect to previously defined climatic variation. In the LLZAD₉₉ model a number of major soils are correlated to periods defined as glaciations in the oceanic $\delta^{18}\text{O}$ record and a number of loess units are associated to periods known to coincide with interglacials.

2. Target curves and tuning procedure

In the present study (hereafter referred to as HLD₀₀) two loess profiles were selected to provide proxy-climate reference data for orbital tuning. The first profile was constructed from particle

size data from the Baoji section (34.2°N, 107.0°E) reported by Ding et al. [9] and the second profile consisted of χ measurements from Luochuan (35.8°N, 109.2°E) reported by Lu et al. [16].

In any orbital tuning process the selection of a suitable astronomical solution to act as a target curve is critical. Orbital timescale evaluation by Lourens et al. [18] demonstrated that the astronomical solution of Laskar [1] calculated with present-day input values for the dynamical ellipticity of the Earth and tidal dissipation by the Sun and Moon produced an accurate solution (hereafter referred to as La_{90(1,1)}) with respect to the geological record. On the basis of the Lourens et al. [18] investigation, the La_{90(1,1)} 65°N summer insolation curve was selected as the primary target curve for this study. The 65°N insolation was selected over a lower latitude curve because of its increased expression of obliquity and from the evidence of previous investigations [15,18,19], which have shown the reliability of the La_{90(1,1)} 65°N summer insolation curve in the orbital tuning of Mediterranean palaeoclimatic schemes (located on a similar latitude to the Chinese loess Plateau).

Previous authors have proposed that in the past the climate of the loess plateau region was primarily driven by mechanisms responding to fluctuations in Northern Hemisphere ice volume via a transcontinental teleconnection controlled by the westerlies and the positioning of the Siberian–Mongolian High [7,20–22]. In response to in-

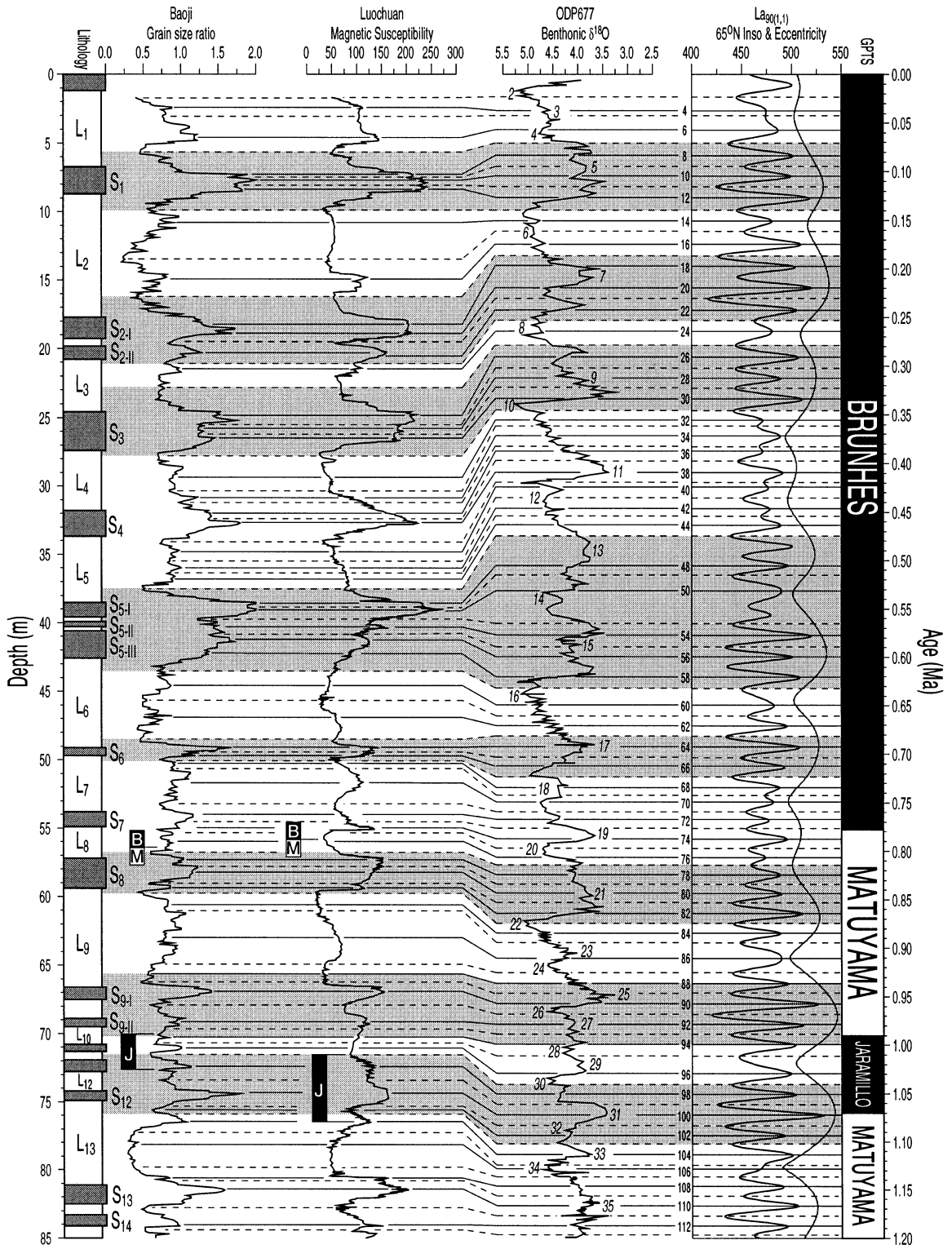


Fig. 2

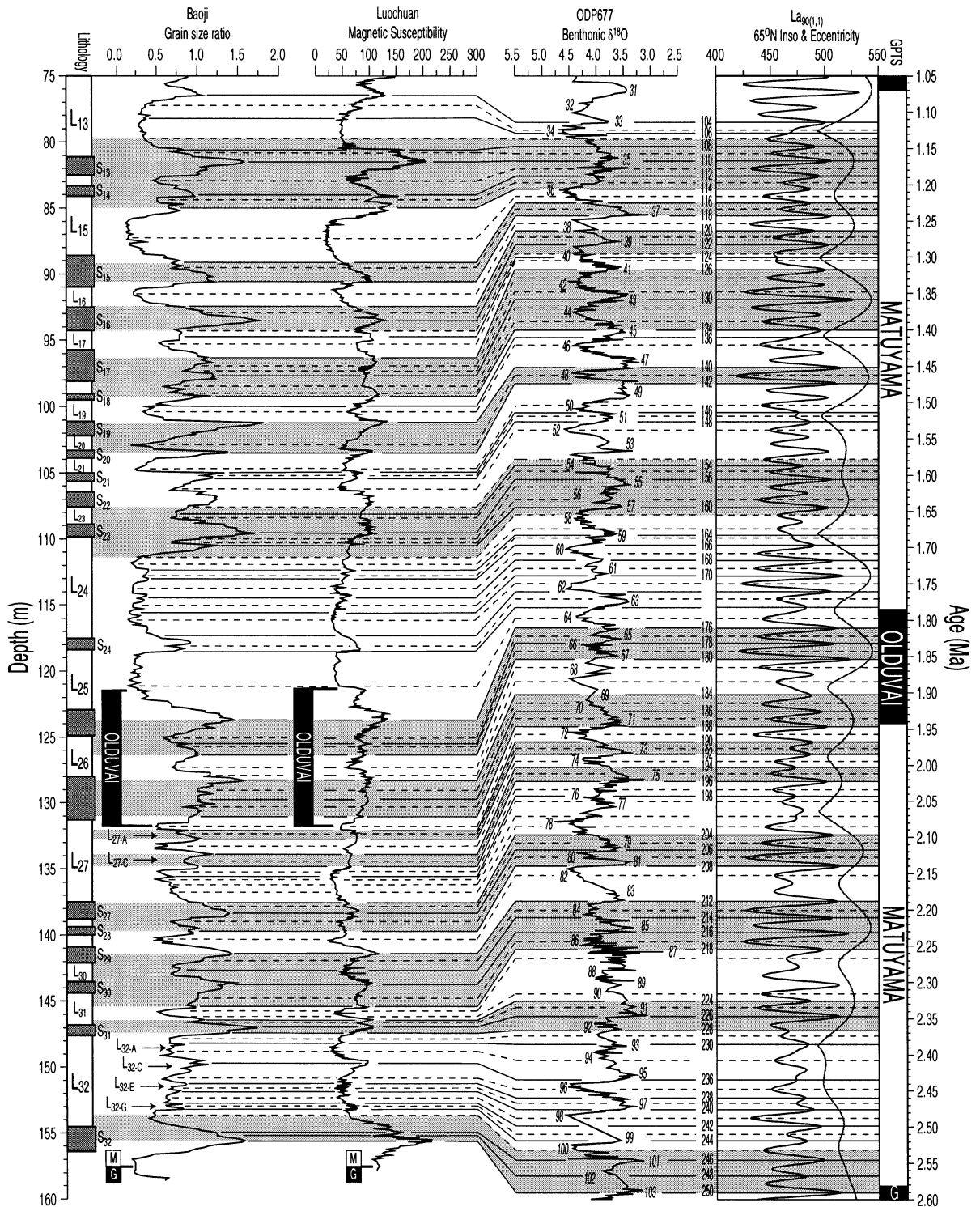


Fig. 2 (continued).

Fig. 2. Correlation of the records of Baoji grain size ratio (GSR) and Luochuan magnetic susceptibility χ (fitted to the Baoji depth scale) to the 65°N $La_{90(1,1)}$ insolation curve [1] (i-cycle numbers shown to the left) and ODP677 benthonic $\delta^{18}O$ record [2] (MIS numbers shown adjacent to curve). The $La_{90(1,1)}$ eccentricity component is displayed for comparison with the longer-term trends observed within the loess record. Correlation points linking warm (cold) features are shown as solid (dashed) lines. The palaeomagnetic record for the Baoji section was constructed by Rutter et al. [31] and can be compared to the geomagnetic polarity time scale (GPTS) shown to the right of the diagram [2,18,29,30].

←

creased ice volume, this mechanism would result in a strengthening of the winter monsoon system, an increased loess deposition rate, suppression of the summer monsoon and reduced pedogenesis. Therefore the relationship between loess accretion and the development of continental ice sheets was evaluated during the HLD₀₀ tuning procedure by comparing the loess records to the orbitally tuned ODP677 $\delta^{18}O$ records of Shackleton et al. [2] in a manner similar to that of Heller and Liu [14].

The tuning procedure adopted in the construction of the HLD₀₀ chronology differed substantially from those of DYRL₉₄ and LLZAD₉₉. It was chosen not to filter the proxy-climate data and therefore the formulation of an initial chronology was not required. The HLD₀₀ chronology was formulated by correlation of the unfiltered proxy-climate records to the $La_{90(1,1)}$ and ODP677 $\delta^{18}O$ curves (features within the insolation record will be referred to using the i-cycle codification of Lourens et al. [18]). To ensure that a consistent relationship between the proxy-climate records and the chosen target curves was maintained throughout the tuning procedure a number of correlation criteria were imposed. Palaeosols were related to regional maxima in insolation, maxima in eccentricity and odd numbered marine oxygen isotope stages (MIS), whilst loess units were consistently assigned to insolation minima and evenly numbered MIS. The HLD₀₀ scheme follows the method of Shackleton et al. [2], which utilised a zero time lag between insolation forcing and response of the climate system.

Displaced palaeomagnetic signals were considered to be a major factor in the construction of the HLD₀₀ chronology. The timescale was therefore constructed so that the positions of the palaeomagnetic reversals within the loess sequences corresponded to ages identical to or older than the accepted reversal ages (see Table 1 for control ages).

3. Orbital tuning

To ensure a consistent correlation the selected sections were initially cross-correlated in the depth domain. The correlation was a relatively simple procedure involving a downward matching of recognised units within the profiles (loess and soil units are defined using a sequential nomenclature of S_{xx} and L_{xx} respectively).

3.1. S_0 – L_5

Between the Holocene soil, S_0 , and the base of loess unit, L_5 , the proposed HLD₀₀ age model is identical to those proposed by a number of previous workers [16,17,22] (albeit for the presence of slight discrepancies due to minor chronological differences in the $La_{90(1,1)}$ and Berger and Loutre [23] astronomical solutions, Fig. 2).

3.2. S_5 – L_6

Palaeosol S_5 is a unit composed of subsoils S_{5-I} , S_{5-II} and S_{5-III} , intercalated with two thin loess layers L_{5-II} and L_{5-III} . We correlate the upper portion of S_{5-I} to the period between i-cycles 45–49, associating the top of S_{5-I} to MIS13 within the ODP677 $\delta^{18}O$ record. The lower segment of S_{5-I} and the upper half of L_{5-II} are correlated to i-cycles 49–53, MIS14. The bottom of the S_5 palaeosol complex, from the lower portion of L_{5-II} to the base of S_{5-III} , is related to i-cycles 53–59 and MIS15. Although the choice to correlate the S_5 pedocomplex to three marine isotope stages in preference to a single stage would not seem an obvious one, three lines of evidence support the scheme. Firstly, the ODP677 $\delta^{18}O$ record of Shackleton et al. [2] shows that MIS14 is a subdued and shorter cold period than the other stages in this portion of the marine record. Secondly, spanning the S_5 complex across

MIS13–15 results in a low, uniform accumulation rate as would be expected during palaeosol formation. Thirdly, spanning S_5 solely across MIS13 would ultimately result in the positioning of the Matuyama–Brunhes Boundary above the accepted MIS19 age, therefore violating the correlation criterion of delayed palaeomagnetic signal lock-in. Below S_5 , we correlate the period of winter monsoon domination corresponding to L_6 to the glacial of MIS16 (i-cycles 59–63), which was longer and colder than MIS14.

3.3. S_6 – L_8

Between S_6 and L_8 the structure of the loess record is consistent with the pattern described in the marine record. S_6 in the HLD₀₀ correlation is placed between i-cycles 63–67, assigning the palaeosol a duration of ~ 20 kyr and associating the enhanced levels of pedogenesis to MIS17. L_7 is correlated to i-cycles 67–71 and MIS18, whilst palaeosol S_7 is fitted to i-cycles 72–74 and MIS19. Below S_7 the HLD₀₀ correlation matches L_8 to i-cycle range 75–77, MIS20.

3.4. S_8 – L_9

S_8 and L_9 are typical of the large-scale units observed in the upper portions of the loess sequences. Palaeosol S_8 is correlated to i-cycles 77–83 and MIS21. L_9 is almost 7 m thick at Baoji and the proxy values towards its midpoint are comparable with those observed within the more weakly developed palaeosols (e.g. S_7). The structure of the L_9 unit suggests that its formation spanned i-cycles 83–89 corresponding to MIS22, 23 and 24. The $\delta^{18}\text{O}$ variation of ODP677 record indicates that MIS23 was a relatively subdued warm phase, supporting the hypothesis that the stage was recorded only as a zone of relatively high proxy values within L_9 .

3.5. S_9 – S_{12}

A complex consisting of five palaeosols (S_{9-I} , S_{9-II} , S_{10} , S_{11} , S_{12}) occurs beneath L_9 . The complex is bounded by two major soils, S_{9-I} and S_{12} , whilst S_{9-II} , S_{10} and S_{11} are only weakly devel-

oped. Comparison to ODP677 shows a similar pattern in the marine record, with MIS25 and MIS31 bounding the weaker stages MIS27 and MIS29. This correspondence allows S_{9-I} and S_{12} to be correlated to MIS25 and 31 respectively, whilst S_{9-II} and S_{10} are fitted to MIS27 and 29 respectively, with S_{11} matched to a warm phase in the MIS31/30 transition (corresponding to i-cycle 98). The shoulder in the insolation curve at i-cycle 104 is linked to the well-developed horizon located below the S_{12}/L_{13} palaeosol–loess transition.

At the point of the lower Jaramillo in the Baoji section the discussed S_{9-I} – S_{12} match would appear to violate the palaeomagnetic criterion of placing reversal boundaries on or below their reference age. Close inspection reveals that the locations of the Jaramillo subchron differ substantially in the Baoji and Luochuan sections, spanning L_{10} – S_{12} at Baoji and L_{11} – L_{13} at Luochuan. In this situation we violated the correlation criteria for two reasons. Firstly, the fitting of S_{9-I} and S_{12} to MIS25 and 31 provides a very convincing match for the top and base of the pedocomplex. Secondly, the Baoji palaeomagnetic record appears to contain a number of normally magnetised samples within reversed polarity zones, indicating that the viscous overprint of the samples may have not always been successfully removed, resulting in the possible misidentification of reversal boundary locations [24].

3.6. L_{13} – L_{15}

The preceding correlation of S_{12} to the $La_{90(1,1)}$ insolation curve had placed the top of L_{13} at i-cycle 101 and we therefore assigned the loess unit to MIS32, 33 and 34. The structure of MIS35 consists of a substantial triple-peaked warm phase, commencing after the gradual termination of MIS36. The large-scale structure of MIS36, 35 and 34 indicates that stages 34 and 36 correspond to units L_{13} and L_{15} respectively, whilst the S_{13} – L_{14} – S_{14} complex was formed during MIS35 with the thin intervening loess unit (L_{14}) deposited during the cooling episode located at the midpoint of the warm stage at ~ 1.175 Ma.

3.7. S_{15} – S_{23}

S_{15} and S_{16} are correlated across i-cycles 116–118 (MIS37) and 120–123 (MIS39) respectively. The thick palaeosol S_{17} contains a double peak, which is correlated to span i-cycles 126–131; this places the upper peak of S_{17} across i-cycles 126–127 (MIS41) and therefore the lower peak to i-cycles 129–131 (MIS43). S_{18} is weakly developed and is correlated to i-cycle 134 (MIS45). S_{19} is correlated to i-cycle 140, associating the palaeosol formation to the substantial warm phase of MIS47, with the surrounding loess units L_{20} and L_{19} assigned to the cold episodes MIS48 and 46 respectively. Palaeosol S_{20} has a similar structure to S_{19} and is correlated to i-cycles 142–144, corresponding to MIS49.

S_{21} and S_{22} are palaeosols superimposed upon a background of well-developed loess. S_{21} and S_{22} are each correlated to two peaks in insolation, resulting in their association to i-cycles 146–148 (MIS51) and 150–152 (MIS53) respectively.

3.8. S_{23} – S_{24}

Slightly below the L_{24}/S_{23} transition the loess curves indicate the presence of a developed horizon recorded in the upper portion of the L_{24} loess unit. Following the correlation of the overlying portion of the loess sequence, palaeosol S_{23} must be associated to i-cycles 155–157 (MIS55). The ODP677 benthonic $\delta^{18}\text{O}$ record indicates that both MIS56 and 57 were episodes of a short duration. This $\delta^{18}\text{O}$ structure would suggest that the developed horizon at the top of L_{24} and the overlying trough at the point of the L_{24}/S_{23} transition should be assigned to MIS57 and 56 respectively (i-cycles 160 and 157–159). The detailed structure of loess unit L_{24} is clearly defined in the median grain size (MGS) record from the Baoji section (Fig. 3). The MGS curve displays three main periods of increased grain size (L_{24-B} , L_{24-D} , L_{24-F}). The triple-trough structure of L_{24} provides a coherent fit with the ODP677 $\delta^{18}\text{O}$ variation reported between MIS58 and 62 (i-cycles 161–171). Peaks within the ODP677 $\delta^{18}\text{O}$ benthonic record corresponding to the warm MIS59 and 61 episodes are of a low amplitude and in the

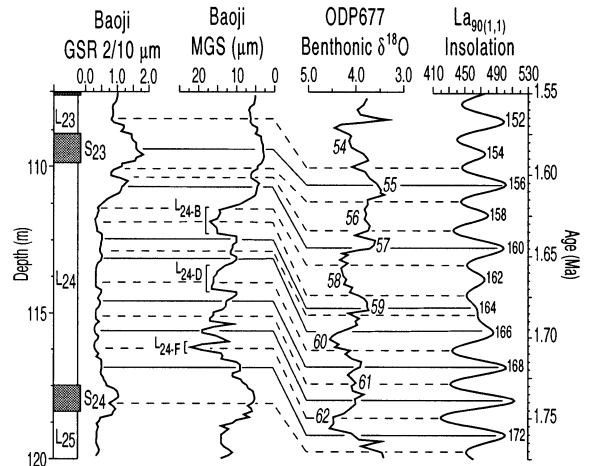


Fig. 3. Analysis of the Baoji S_{23} – S_{25} complex utilising GSR and median grain size (MGS) curves in order to define the fine-scale proxy-climatic pattern recorded in the loess units and correlate the sequence to the benthonic ODP677 $\delta^{18}\text{O}$ records (the MGS axis has been inverted to show particle size variation in the same sense as the GSR data).

sister $\delta^{18}\text{O}$ planktonic record the same stages are indistinct against the background of the cold MIS58, 60 and 62 climate. Preceding the commencement of the MIS58–62 cold phase there was a substantial warm stage, MIS63. We relate MIS63 (i-cycles 172–174) to the weakly developed palaeosol S_{24} . With the upper portion of L_{24} assigned to MIS57 and S_{24} correlated to MIS63, we assign the three features of increased MGS recorded in the body of L_{24} to MIS58, 60 and 62 (and i-cycles 161–163, 167 and 171 respectively). The two recorded periods of reduced MGS within L_{24} must therefore correspond to MIS59 and 61 (i-cycle ranges 164–166 and 168–170 respectively).

3.9. L_{25} – L_{26}

Analysis of the ODP677 $\delta^{18}\text{O}$ curve indicates that MIS64 was an episode of substantial duration, separating the high-magnitude warm peaks of MIS63 and 65. The presence of a long and cold isotope stage at this point suggests that unlike L_{24} , L_{25} corresponds to a single cold event, MIS64 (i-cycles 174–175). The underlying palaeosol S_{25} is fitted to the double peak of MIS65 (i-cycles 176–178). MIS66, 67 and 68 are all weak

and of relatively short duration. L_{26} shows substantially greater background GSR and χ values than the previously discussed L_{24} and L_{25} units, and additionally contains a proto-soil approximately at its centre. Therefore unit L_{26} is correlated to the weak episodes MIS66, 67 and 68 (i-cycles 178–183).

3.10. S_{26} – L_{27}

The upper horizon of S_{26} is dominated by a peak, whilst the lower portion of the palaeosol unit consists of well-developed sediments overlying the L_{27}/S_{26} transition. The dominant peak of the S_{26} unit is correlated to MIS69 (i-cycle 184) and the middle portion of the palaeosol is attributed to MIS70 (i-cycle 185). On the basis of the above correlation, the lower portion of the S_{26} unit is assigned to MIS71 (i-cycles 186–188).

Loess unit L_{27} contains two double-peaked features, designated as L_{27-A} and L_{27-C} . Comparison of these structures to the ODP677 record, suggests that the upper L_{27-A} feature corresponds to warm episode MIS73 (i-cycles 190–192) and the peaks of the lower L_{27-C} feature correspond to MIS75 (i-cycles 194–196). Therefore the entire L_{27} unit is correlated to span the time period between MIS72 and 78 (i-cycle range 189–203).

3.11. S_{27} – S_{31}

The S_{27} – S_{31} palaeosol complex is composed of four well-developed soils and a weaker horizon, S_{28} . In the uppermost portion of the complex, S_{27} is correlated to MIS79 (i-cycles 204–206) and the weaker S_{28} unit is assigned to the short duration MIS81 episode (i-cycle 208). The HLD₀₀ correlation therefore results in the L_{28} loess unit corresponding to MIS80 (i-cycle 207). The ODP677 record shows MIS82 (i-cycles 209–211) to be a substantial cold period and this corresponds with the low GSR and χ values of L_{29} . S_{29} is correlated to the broad MIS83 episode (i-cycle 212) and the underlying loess unit L_{30} is attributed to cold MIS84 (i-cycles 213–214).

The upper portion of S_{30} contains a major peak and at the S_{30}/L_{31} transition the sediments are well developed with high proxy values observed

in the upper half of L_{31} . At the midpoint of L_{31} there is a major trough that occurs above a small peak and trough feature marking the S_{31}/L_{31} transition. The combined structure of the adjacent S_{30} and L_{31} units suggests that the major peak contained within S_{30} corresponds to MIS85 (i-cycles 214–216), whilst the developed loess at the top of L_{31} is related to MIS87 (i-cycle 218). The trough observed at the midpoint of L_{31} is assigned to MIS88 and the very weak MIS89 (i-cycles 219–223). S_{31} is correlated to the major warm event MIS91 (i-cycles 224–226) and the L_{32}/S_{31} transition is therefore assigned to MIS92 (i-cycle 229).

3.12. L_{32} – L_{33}

L_{32} appears to contain four horizons that are developed to a slightly greater extent than the background loess (these ‘warm’ features are designated L_{32-A} , L_{32-C} , L_{32-E} , and L_{32-G} , Fig. 2). Analysis of the ODP677 record below MIS92 demonstrates that from the time of the maximum warm peak in MIS95 there was a gradual but extended period of cooling which encompassed MIS94, 93 and 92. Comparison of this cooling structure to the Baoji GSR record suggests that the peak of feature L_{32-C} corresponds to the peak of MIS95 (i-cycle 236), whilst L_{32-A} corresponds to the weak episode MIS93 (i-cycle 230). The structure of S_{32} clearly indicates that the palaeosol unit should be correlated across MIS101–103 (i-cycles 246–251) and therefore the HLD₀₀ correlation of L_{32-E} and L_{32-G} can be constrained by the peak of L_{32-C} at MIS95 and the L_{32}/S_{32} transition at MIS100. With these correlated boundaries in place, it becomes clear that L_{32-E} and L_{32-G} must be assigned to MIS97 and 99 respectively (i-cycle ranges 238–240, 242–244).

The analysis of a loess section and underlying red-clay sequence at Lingtai (35°01'N, 107°31'E) by Ding et al. [25] shows an increase in magnetic susceptibility below L_{33} to values comparable with those found in S_{32} (MIS101–103). Comparison of this structure to the $\delta^{18}O$ record constructed by Shackleton et al. [26] from ODP846 (3°N, 90°W) indicates that L_{33} was deposited during MIS104 and the underlying increase in magnetic susceptibility was a product of MIS105.

4. Evolutive cross-spectral analysis

Cross-spectral analysis was performed to investigate the coherency between the HLD₀₀ tuned loess records and the La_{90(1,1)} orbital solution in the frequency domain. An evolutive approach was applied in the cross-spectral analysis in order that shifts in coherent frequencies could be localised in time. The evolutive technique utilised a Blackman–Tukey cross-spectral analysis [27] within a 500 kyr window. The window was migrated through each time series in increments of 50 kyr and regions containing frequencies with non-zero coherence levels above 80% and 95% were isolated (Fig. 4). Evolutive phase spectra are not considered because a zero time lag between insolation change and monsoon response had been assumed in the construction of the HLD₀₀ model.

Throughout the Baoji and Luochuan time series, cross-spectral analysis reveals coherent frequencies corresponding to the 41 kyr (0.0244 kyr⁻¹) obliquity cycle. In addition, there is a coherent component within each section corresponding to the sporadic appearance of the 54 kyr (0.0185 kyr⁻¹) obliquity cycle. Consideration of the 23 and 19 kyr climatic components (frequencies of 0.0435 and 0.0526 kyr⁻¹ respectively) shows the presence of coherent precession signals throughout each of the sections.

The topography of the coherent frequencies in the loess sections gives a clear indication that orbital frequencies contained within the chosen target curves have been introduced successfully into the Chinese loess records by tuning them to the HLD₀₀ solution.

There is no eccentricity component present within the topography of cross-spectral analysis. The absence of this signal is expected because the direct contribution of eccentricity to insolation variation is <0.1%. The main influence that eccentricity exerts on radiation change is by modulation of the precession signal [28], a mechanism which will not be detected by cross-spectral analysis.

5. Comparison of HLD₀₀ and LLZAD₉₉ solutions

Comparison of the HLD₀₀ scheme to the recently published LLZAD₉₉ model, shows that the HLD₀₀ model is the more consistent of the two chronologies with respect to the known mechanisms of loess accumulation and post-depositional alteration. One example of how the HLD₀₀ model appears to improve on the LLZAD₉₉ scheme occurs in their relative treatment of the S₁₃–S₁₄ region of the loess sequences.

L₁₃ is a unit with a thickness of ~6 m (in the

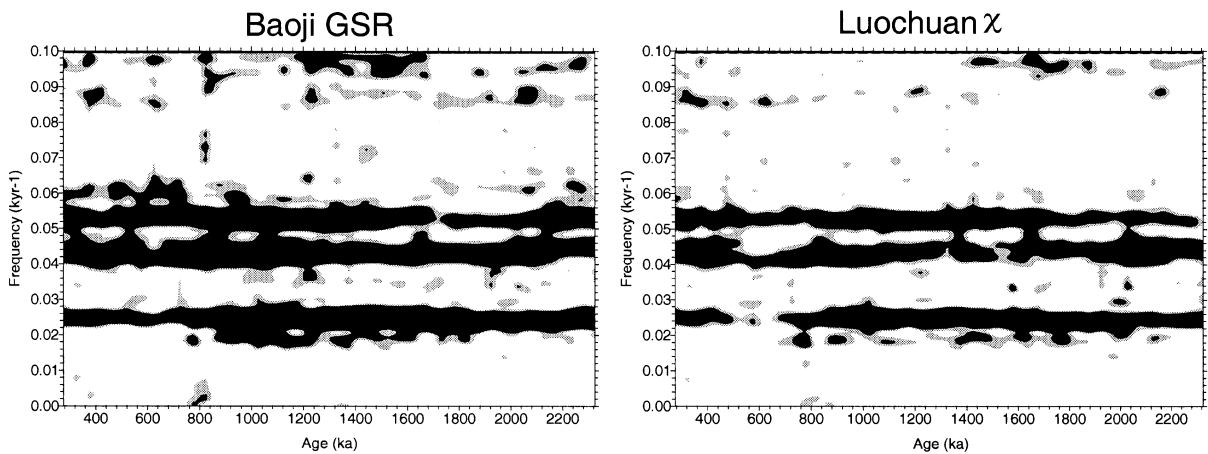


Fig. 4. Evolutive cross-spectral analysis to isolate and localise in the time domain coherent frequencies in the La_{90(1,1)} insolation and HLD₀₀ loess time series. Frequencies above the level of 80% non-zero coherence are shown in grey, whilst frequencies above the 95% level are shown in black.

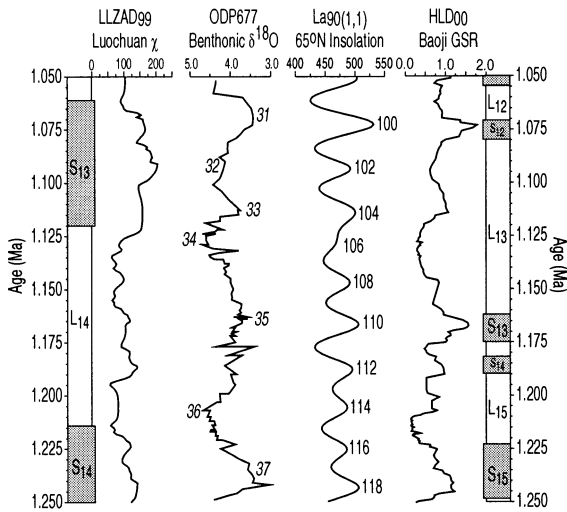


Fig. 5. Comparative structures of the LLZAD₉₉ and HLD₀₀ orbital solutions through the S₁₃–S₁₄ soil couplet, demonstrating the consistency of the HLD₀₀ model with respect to both the insolation record and marine isotope curve.

Baoji section), which is correlated to i-cycles 95–97 in the LLZAD₉₉ model (Fig. 5), therefore proposing that the unit was predominantly deposited during the warm MIS29 episode. Subsequently, the soil couplet consisting of S₁₃, L₁₄ and S₁₄ is associated to MIS31–38 in the LLZAD₉₉ correlation, resulting in a fit which proposes that L₁₄ was deposited during the long, warm stage MIS35.

The HLD₀₀ model fits the L₁₃–L₁₅ sequence across five isotope stages, MIS32–36. The S₁₃–S₁₄ palaeosol couplet is assigned solely to

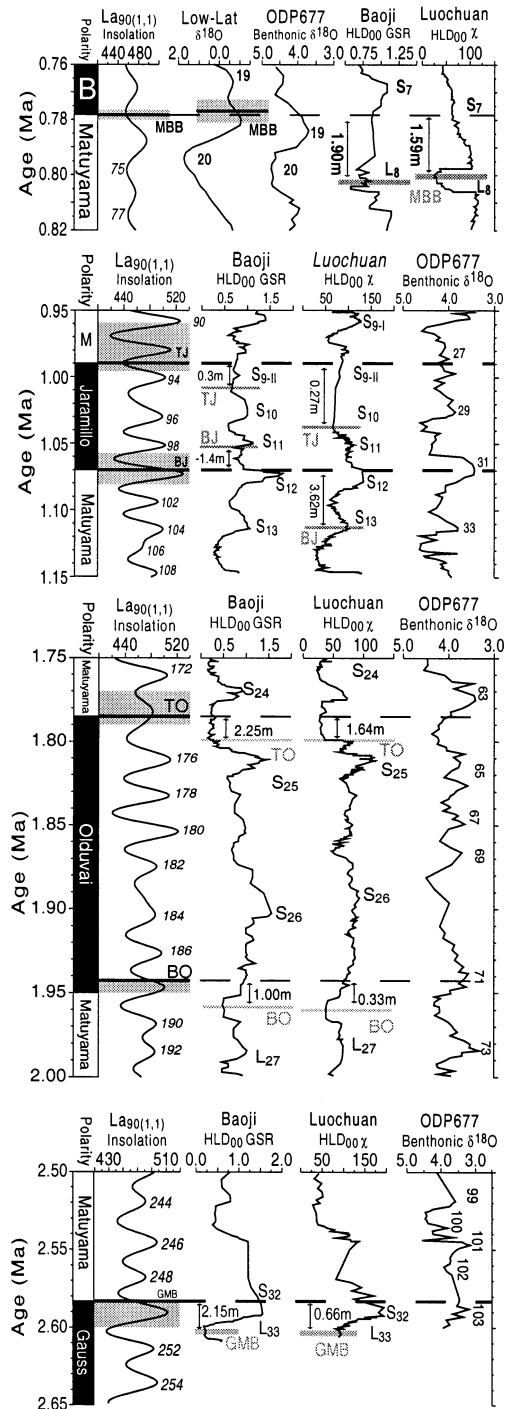


Fig. 6. Comparison of the palaeomagnetic boundary positions in the Baoji and Luochuan sections after tuning to the HLD₀₀ chronology. Both sections show the presence of a significant downward displacement of the palaeomagnetic horizons with respect to the reversal reference ages (displayed on the La_{90(1,1)} insolation data). For purposes of comparison, the stacked low-latitude δ¹⁸O record of Bassinot et al. [32], which contains an alternative astronomical age for the MBB of 0.777 ± 0.004 Ma [29], is shown. In addition, the ODP677 benthonic δ¹⁸O record is included to illustrate the inferred position of the palaeomagnetic boundaries within the tuning target curve. Arrows placed on the Baoji and Luochuan curves indicate the magnitude of the lock-in delay in the depth domain. Gray bars placed on the reference ages of the Jaramillo and Olduvai subchrons and the GMB represent astronomical reversal age ranges based on alternative studies [2,13].

MIS35, which shows a triple-peaked structure similar to the pattern spanning the soil complex and the top of L₁₅. The bounding loess units L₁₃ and L₁₅ are correlated to cold stages MIS32 and 34 (with a region of high GSR loess in L₁₃ matched to the weak MIS33 episode) and MIS36. The example of the S₁₃–S₁₄ complex demonstrates that the use of both insolation and isotope target curves in the development of the HLD₀₀ model resulted in a chronological solution that is consistent both with orbital parameters and known climatic variation.

6. Palaeomagnetic boundaries

The discrepancies between the loess palaeomagnetic boundary positions of the HLD₀₀ model and the accepted reversal ages can provide important information concerning the magnitude of the delay in signal acquisition within the Baoji and Luochuan sections. Since the HLD₀₀ scheme utilises a zero time lag between insolation forcing and monsoon response, the apparent lock-in periods would be reduced if a time lag was imposed.

6.1. Matuyama–Brunhes Boundary (MBB)

Comparison of the orbital ages derived for the positions of the MBB in the HLD₀₀ tuned Baoji and Luochuan sections to the MBB age of 0.778 ± 0.0017 Ma [29], indicates that the acquisition of a stable palaeomagnetic signal was delayed in the loess records (Fig. 6, Table 1). The MBB within the Baoji and Luochuan sections is delayed by periods of ~ 26 kyr and ~ 23 kyr respectively. The corresponding lock-in depths of ~ 1.90 m in the Baoji section and ~ 1.59 m in the Luochuan section are comparable to the lock-in depth range proposed by Zhou and Shackleton [17].

6.2. Jaramillo subchron

The Baoji and Luochuan sequences display a substantial disparity in their recording of the Jaramillo subchron (Fig. 6). The top of the subchron is displaced by ~ 0.30 m and ~ 0.27 m within the Baoji and Luochuan records, respectively, corre-

sponding to periods of ~ 6 kyr (Baoji) and ~ 47 kyr (Luochuan) records. Scrutiny of the Baoji and Luochuan records indicates that the substantial difference in the lock-in periods is caused by differences in the published positions of the palaeomagnetic boundaries within the stratigraphic schemes. The correlation problems experienced in the region of the lower Jaramillo are increased by the uncertainties associated with the boundary reference age [2]. Because of the correlation of S₁₂ to MIS31, the base of the Jaramillo in the Baoji section must be assigned a negative lock-in, whilst the position of the boundary at Luochuan gives a lock-in of ~ 3.62 m, corresponding to ~ 43 kyr.

6.3. Olduvai subchron

Both the Baoji and Luochuan sections display a consistent delay of ~ 10 – 20 kyr in the formation of stable NRM signals corresponding to the Olduvai subchron (Fig. 6). In the Baoji section the top and base of the Olduvai have lock-in depths of ~ 2.25 m and ~ 1.00 m respectively, whilst in the Luochuan record the same horizons have lock-in depths of ~ 1.64 and ~ 0.33 m respectively.

6.4. Gauss–Matuyama Boundary (GMB)

Both loess records display displaced palaeomagnetic signals with respect to the GMB reference age of 2.582 Ma (MIS103) determined by Langereis et al. [30]. The sequences display lock-in periods and depths that are consistent with the previously discussed palaeomagnetic boundaries, ~ 21 kyr and ~ 2.15 m in the Baoji section and ~ 20 kyr and ~ 0.66 m in the Luochuan section (Fig. 6).

7. Conclusions

We have formulated a new Chinese loess chronology using summer and winter monsoon proxies tuned to target curves that represent both direct solar forcing and global ice volume. A number of conclusions can be drawn from the HLD₀₀ scheme:

Table A1

Stratigraphic marker	Depth (m)	Age (Ma)	Stratigraphic marker	Depth (m)	Age (Ma)
Top of S1	6.70	0.079	Top of S15	88.60	1.223
Base of S1	8.70	0.129	Base of S15	91.00	1.249
Top of S2-I	17.70	0.196	Top of S16	92.50	1.263
Base of S2-I	19.30	0.226	Base of S16	94.25	1.296
Top of S2-II	19.80	0.234	Top of S17	95.70	1.311
Base of S2-II	20.80	0.250	Base of S17	98.10	1.363
Top of S3	24.60	0.290	Top of S18	99.00	1.386
Base of S3	27.40	0.342	Base of S18	99.50	1.405
Top of S4	31.80	0.386	Top of S19	101.10	1.448
Base of S4	33.70	0.417	Base of S19	102.20	1.458
Top of S5-I	38.50	0.503	Top of S20	103.30	1.470
Base of S5-I	39.60	0.556	Base of S20	103.90	1.484
Top of S5-II	39.90	0.568	Top of S21	105.00	1.514
Base of S5-II	40.30	0.575	Base of S21	105.65	1.530
Top of S5-III	40.60	0.581	Top of S22	106.40	1.541
Base of S5-III	42.60	0.625	Base of S22	107.60	1.573
Top of S6	49.10	0.693	Top of S23	108.90	1.600
Base of S6	49.70	0.713	Base of S23	109.90	1.614
Top of S7	53.80	0.765	Top of S24	117.50	1.767
Base of S7	54.90	0.788	Base of S24	118.40	1.774
Top of S8	57.20	0.807	Top of S25	122.90	1.807
Base of S8	59.40	0.865	Base of S25	124.90	1.820
Top of S9-I	66.60	0.952	Top of S26	128.00	1.885
Base of S9-I	67.50	0.964	Base of S26	131.30	1.949
Top of S9-II	68.90	0.977	Top of S27	137.50	2.095
Base of S9-II	69.50	0.984	Base of S27	138.80	2.125
Top of S10	70.80	1.012	Top of S28	139.40	2.135
Base of S10	71.30	1.034	Base of S28	140.00	2.147
Top of S11	71.95	1.044	Top of S29	140.90	2.172
Base of S11	72.80	1.055	Base of S29	142.10	2.204
Top of S12	74.20	1.071	Top of S30	143.50	2.230
Base of S12	74.90	1.080	Base of S30	144.40	2.240
Top of S13	81.10	1.162	Top of S31	146.80	2.341
Base of S13	82.50	1.175	Base of S31	147.60	2.369
Top of S14	83.30	1.182	Top of S32	154.50	2.540
Base of S14	84.10	1.190	Base of S32	156.40	2.596

1. The formulation of an orbitally tuned palaeoclimatic timescale, based on the assumptions that loess units correspond to regions of insolation minima/even numbered MIS and palaeosols to regions of insolation maxima/odd numbered MIS, provides a robust, high-resolution chronological solution for the Chinese loess sequences. The HLD₀₀ chronology enables the precise correlation of the terrestrial loess record to the marine climatic record.
2. The ability to formulate an accurate correlation of the loess climatic record to the marine realm indicates that grain size parameters and magnetic susceptibility variations recorded in Chinese loess deposits provide reliable proxy data for winter and summer monsoon activity. These parameters provide a consistent Quaternary climatic history for sites located in the central and southern regions of the Chinese loess plateau.
3. The studied loess sections display, in both the palaeosol and loess units, the presence of a substantial delay in the acquisition of a stable palaeomagnetic signal. Although the precise

mechanism responsible for this delay has not been determined, the consideration of such a process is essential in future investigations of the loess palaeomagnetic archive.

4. Cross-spectral analysis provides a powerful tool in determining whether coherent orbital frequencies have successfully been introduced into a palaeoclimatic time series during a tuning procedure. Additionally, the use of an evolutive method during the analysis allows time localisation of the frequency signal.

Acknowledgements

The authors are grateful to H. Lu for providing access to the original Luochuan data set and F. Heller and L.P. Zhou for helpful reviews. This work was conducted under the programme of the Vening Meinesz Research School of Geodynamics (VMSG). [RV]

Appendix A. Astronomical ages

Astronomical ages derived from the HLD₀₀ model for each of the identified Baoji units are presented in Table A1.

References

- [1] J. Laskar, The chaotic motion of the solar system: A numerical estimate of the size of the chaotic zones, *Icarus* 88 (1990) 266–291.
- [2] N.J. Shackleton, A. Berger, W.R. Peltier, An alternative astronomical calibration of the lower Pleistocene timescale based on ODP site 677, *Trans. R. Soc. Edinb. Earth Sci.* 81 (1990) 251–261.
- [3] J. Xiao, S.C. Porter, Z. An, Grain size of quartz as an indicator of winter monsoon strength on the loess plateau of Central China during the last 130,000 yr, *Quat. Res.* 43 (1995) 22–29.
- [4] E. Derbyshire, R.A. Kemp, X. Meng, Climate change, loess and palaeosols: proxy measures and resolution in North China, *J. Geol. Soc. Lond.* 154 (1997) 793–805.
- [5] L.P. Zhou, F. Oldfield, A.G. Wintle, S.G. Robinson, J.T. Wang, Partly pedogenic origin of magnetic variations in Chinese loess, *Nature* 346 (1990) 737–739.
- [6] F. Heller, T. Liu, Magnetism of Chinese loess deposits, *Geophys. J. R. Astron. Soc.* 77 (1984) 125–141.
- [7] J. Bloemendal, X.M. Liu, T.C. Rolph, Correlation of the magnetic susceptibility stratigraphy of Chinese loess and the marine oxygen isotope record, chronological and palaeoclimatic implications, *Earth Planet. Sci. Lett.* 131 (1995) 371–380.
- [8] F.H. Chen, J. Bloemendal, J.M. Wang, J.J. Li, High-resolution multi-proxy climate records from Chinese loess: evidence for rapid climatic changes over the last 75 kyr, *Palaeogeogr. Palaeoclimatol. Palaeoecol.* 130 (1997) 323–335.
- [9] Z. Ding, Z. Yu, N.W. Rutter, T. Liu, Towards an orbital time scale for Chinese loess deposits, *Quat. Sci. Rev.* 13 (1994) 39–70.
- [10] J.D. Hays, J. Imbrie, N.J. Shackleton, Variations in the Earth's orbit pacemaker of the ice ages, *Science* 194 (1976) 1121–1132.
- [11] M.E. Raymo, W.F. Ruddiman, J. Blackman, B.M. Clement, D.G. Martinson, Late Pliocene variations in Northern Hemisphere ice sheet and North Atlantic Deep Water circulation, *Paleoceanography* 4 (1989) 413–446.
- [12] W.F. Ruddiman, M.E. Raymo, D.G. Martinson, B.M. Clement, J. Backman, Pleistocene Evolution: Northern hemisphere ice sheets and North Atlantic Ocean, *Paleoceanography* 4 (1989) 353–412.
- [13] F.J. Hilgen, Astronomical calibration of Gauss to Matuyama sapropels in the Mediterranean and implication for the Geomagnetic Polarity Time Scale, *Earth Planet. Sci. Lett.* 104 (1991) 226–244.
- [14] F. Heller, T.S. Liu, Palaeoclimatic and sedimentary history from magnetic susceptibility of loess in China, *Geophys. Res. Lett.* 13 (1986) 1169–1172.
- [15] N. van Vugt, J. Steenbrink, C.G. Langereis, F.J. Hilgen, J.E. Meulenkamp, Magnetostratigraphy-based astronomical tuning of the early Pliocene lacustrine sediments of Ptolemais (NW Greece) and bed-to-bed correlation with the marine record, *Earth Planet. Sci. Lett.* 164 (1998) 535–551.
- [16] H. Lu, X. Liu, F. Zhang, Z. An, J. Dodson, Astronomical calibration of loess-paleosol deposits at Luochuan central Chinese loess plateau, *Palaeogeogr. Palaeoclimatol. Palaeoecol.* 154 (1999) 237–246.
- [17] L.P. Zhou, N.J. Shackleton, Misleading positions of geomagnetic reversal boundaries in Eurasian loess and implications for correlation between continental and marine sedimentary sequences, *Earth Planet. Sci. Lett.* 168 (1999) 117–130.
- [18] L.J. Lourens, A. Antonarakou, F.J. Hilgen, A.A.M. van Hoof, C. Vergnaud-Grazzini, W.J. Zachariasse, Evaluation of the Plio-Pleistocene astronomical timescale, *Paleoceanography* 11 (1996) 391–413.
- [19] C.G. Langereis, M.J. Dekkers, G.J. de Lange, M. Paterne, P.J.M. van Santvoort, Magnetostratigraphy and astronomical calibration of the last 1.1 Myr from an eastern Mediterranean piston core and dating of short events in the Brunhes, *Geophys. J. Int.* 129 (1997) 75–94.

- [20] Z. Ding, T. Liu, N.W. Rutter, Z. Yu, Z. Guo, R. Zhu, Ice-Volume forcing of east Asian winter monsoon variations in the past 800,000 years, *Quat. Res.* 44 (1995) 149–159.
- [21] S.C. Porter, Z. An, Correlation between climate events in the North Atlantic and China during the last glaciation, *Nature* 375 (1995) 305–308.
- [22] N.J. Shackleton, Z. An, A.E. Dodonov, J. Gavin, G.J. Kukla, V.A. Ranov, L.P. Zhou, Accumulation rate of loess in Tajikistan and China: Relationship with global ice volume cycles, *Quat. Proc.* 4 (1995) 1–6.
- [23] A. Berger, M.F. Loutre, Insolation values for the climate of the last 10 million years, *Quat. Sci. Rev.* 10 (1991) 297–317.
- [24] F. Heller, M.E. Evans, Loess magnetism, *Rev. Geophys.* 33 (1995) 211–240.
- [25] Z.L. Ding, S.F. Xiong, J.M. Sun, S.L. Yang, Z.Y. Gu, T.S. Liu, Pedostratigraphy and palaeomagnetism of a ~7.0 Ma eolian loess-red clay sequence at Lingtai, Loess Plateau, north-central China and the implications for palaeomonsoon evolution, *Palaeogeogr. Palaeoclimatol. Palaeoecol.* 152 (1999) 49–66.
- [26] N.J. Shackleton, M.A. Hall, D. Pate, Pliocene stable isotope stratigraphy of ODP site 846, *Proc. ODP Sci. Res.* 138 (1995) 337–353.
- [27] D. Paillard, L. Labeyrie, P. Yiou, Macintosh program performs time-series analysis, *EOS* 77 (1996) 379.
- [28] S.C. Clemens, R. Tiedemann, Eccentricity forcing of Pliocene-Early Pleistocene climate revealed in a marine oxygen-isotope record, *Nature* 385 (1997) 801–804.
- [29] L. Tauxe, T. Herbert, N.J. Shackleton, Y.S. Kok, Astronomical calibration of the Matuyama-Brunhes boundary: Consequences for magnetic remanence acquisition in marine carbonates and Asian loess sequences, *Earth Planet. Sci. Lett.* 140 (1996) 133–146.
- [30] C.G. Langereis, A.A.M.V. Hoof, F.J. Hilgen, Steadying the rates, *Nature* 369 (1994) 615.
- [31] N.W. Rutter, Z.L. Ding, M.E. Evans, Y.C. Wang, Magnetostratigraphy of the Baoji loess-paleosol section in the north-central China Loess Plateau, *Quat. Int.* 7/8 (1991) 97–102.
- [32] F. Bassinot, L. Labeyrie, E. Vincent, X. Quidelleur, N. Shackleton, Y. Lancelot, The astronomical theory of climate and the age of the Brunhes-Matuyama magnetic reversal, *Earth Planet. Sci. Lett.* 126 (1994) 91–108.
- [33] W.B. Harland, A.V. Cox, P.G. Llewellyn, C.A.G. Pickton, A.G. Smith, R. Walters, *A Geological Time Scale*, Cambridge University Press, Cambridge, 1982.
- [34] S.C. Cande, D.V. Kent, A new geomagnetic polarity time scale for the late Cretaceous and Cenozoic, *J. Geophys. Res.* 97 (1992) 13917–13951.